

First observations of foreshock bubbles upstream of Earth's bow shock: Characteristics and comparisons to HFAs

D. L. Turner,^{1,2} N. Omid,³ D. G. Sibeck,⁴ and V. Angelopoulos^{1,2}

Received 19 July 2012; revised 4 January 2013; accepted 20 February 2013; published 22 April 2013.

[1] Using multipoint in situ observations upstream of Earth's bow shock from the THEMIS mission, we present the first observations of foreshock bubbles (FBs) and compare them to observations of hot flow anomalies (HFAs). FBs are recently conceptualized kinetic phenomena that can form under the commonplace condition of a rotational discontinuity in the interplanetary magnetic field interacting with backstreaming energetic ions in Earth's quasi-parallel foreshock. FBs may have remained elusive until now due to their many observational similarities to HFAs and the lack of coordinated multipoint measurements. Here we introduce identification criteria for distinguishing between HFAs and FBs using in situ observations, and use them to analyze five example events that occurred on Bastille Day (14 July) and 11–12 August 2008. Three of these events satisfy the criteria for FBs and are inconsistent with multiple criteria for HFAs. The remaining two events are consistent with the traditional picture of HFAs. Furthermore, FBs involve two converging shocks, and using these events, we demonstrate their effectiveness at particle acceleration. Considering that their formation conditions are not extraordinary, FBs may be ubiquitous at collisionless, quasi-parallel shocks in a variety of astrophysical settings.

Citation: Turner, D. L., N. Omid, D. G. Sibeck, and V. Angelopoulos (2013), First observations of foreshock bubbles upstream of Earth's bow shock: Characteristics and comparisons to HFAs, *J. Geophys. Res. Space Physics*, 118, 1552–1570, doi:10.1002/jgra.50198.

1. Introduction

[2] Like other collisionless astrophysical shocks, Earth's bow shock is an effective accelerator of energetic particles via shock-drift and/or Fermi acceleration processes [Scholer *et al.*, 1998; Giacalone, 1992]. When the interplanetary magnetic field (IMF) is quasi-parallel (i.e., $\theta_{BN} < \sim 40^\circ$ [Eastwood *et al.*, 2005]) to the bow shock normal direction, a significant percentage of incident ions and electrons are accelerated and reflected at the shock and travel back upstream along magnetic field lines while drifting due to the convection electric field. These hot, backstreaming particles create kinetic instabilities within the incident solar wind plasma, generating waves that result in additional particle scattering. Nonlinear wave growth and steepening also occur in this region, sometimes forming short large-amplitude magnetic structures [e.g., Schwartz and Burgess, 1991]. This upstream region of energetic ions and waves is known as the ion foreshock [Fuselier, 1995; Eastwood *et al.*, 2005]. The

ion energy in the foreshock is enhanced, effectively causing a pressure increase that results in expansion and formation of a compression region. This compression region that forms along the edge of the foreshock is known as the foreshock compressional boundary and is characterized by enhanced magnetic field and density [Sibeck *et al.*, 2008; Omid *et al.*, 2009].

[3] The foreshock is not a static region, however; its location and properties vary with ever-changing solar wind conditions. Numerous kinetic phenomena resulting from varying solar wind conditions interacting with the quasi-parallel bow shock have been simulated and observed [e.g., Paschmann *et al.*, 1988; Thomas and Brecht, 1988; Thomsen *et al.*, 1988; Schwartz, 1995; Lin, 1997; Sibeck *et al.*, 2002; Omid and Sibeck, 2007; Eastwood *et al.*, 2008; Zhang *et al.*, 2010]. Examples of such phenomena include: hot flow anomalies (HFAs) [e.g., Schwartz *et al.*, 1985; Thomsen *et al.*, 1986; Paschmann *et al.*, 1988], which form due to kinetic interactions between IMF discontinuities and the quasi-parallel bow shock (see further details in the next section); foreshock cavities [e.g., Sibeck *et al.*, 2002], which are seemingly localized patches of ion foreshock that can form independent of IMF discontinuities; and the recently simulated foreshock bubbles (FBs) [Omid *et al.*, 2010], which are very large-scale kinetic events that form due to interactions between IMF discontinuities and counter-streaming, suprathermal ions in the foreshock (see further details in the next section). These foreshock phenomena are important because they can result in extreme magnetospheric disturbances [e.g., Jacobsen *et al.*, 2009; Turner *et al.*, 2011] and are features of other planetary

¹Department of Earth and Space Sciences, University of California, Los Angeles, California, USA.

²Institute of Geophysics and Planetary Physics, University of California, Los Angeles, California, USA.

³Solana Scientific Inc., Solana Beach, California, USA.

⁴NASA Goddard Space Flight Center, Greenbelt, Maryland, USA.

Corresponding author: D. L. Turner, Institute of Geophysics and Planetary Physics, University of California, Los Angeles, CA, USA. (drew.lawson.turner@gmail.com)

©2013. American Geophysical Union. All Rights Reserved.
2169-9380/13/10.1002/jgra.50198

systems, with reported observations at Venus [Slavin *et al.*, 2009], Mars [Øieroset *et al.*, 2001], and Saturn [Masters *et al.*, 2009].

[4] Here we present unprecedented, multipoint observations of a new foreshock phenomenon, foreshock bubbles, and examine their characteristics. We compare them to several examples of HFAs on the same days as the FBs were observed when there were similar identification conditions in the solar wind. In the next section, we discuss the theory of each of these phenomena and introduce formation criteria for both. The data used for this study are then described, followed by the presentation and analysis of each of the example events. We summarize the results in a discussion of: (1) FBs versus HFAs; (2) how this work clarifies our understanding of these two types of transient foreshock events; and (3) ongoing work on implications for magnetosphere-ionosphere dynamics and particle acceleration in astrophysical plasmas.

2. Current Understanding and Theory

[5] Using hybrid simulations, Omid *et al.* [2010] predicted that FBs form due to kinetic interactions between suprathermal, backstreaming ions and incident solar wind plasma with embedded IMF discontinuities that move through and alter the ion foreshock. The following description of FB qualities is based on the results of Omid *et al.* [2010] and subsequent simulations of FBs (N. Omid, private communications, 2011–2012). IMF discontinuities cause deflections of the backstreaming ions in the foreshock.

Such deflections can result in formation of the FB core, a region of depleted density and magnetic field strength, temperatures up to several orders of magnitude hotter than the upstream plasma, highly deflected and sometimes sunward flows, and in situ ULF wave activity. Figure 1 shows hybrid simulation results of a subsolar FB just before it impacts the bow shock (Figure 1a) and a mature HFA along the bow shock (Figure 1b). The FB core (labeled “FB” in Figure 1a) formation relies on a change in the plasma conditions that backstreaming ions experience upstream of the IMF discontinuity: if this change slows a significant amount of these suprathermal ions with respect to the solar wind frame, then they will build-up just upstream of the discontinuity. Essentially, an FB will form if the influx (i.e., the number of particles counter-streaming against the solar wind into a unit area of the incident discontinuity plane in some unit time) of suprathermal ions on the downstream side of the discontinuity is greater than the out-flux on the upstream side. Figure 2 shows an example scenario in which an FB would be formed due to a change in the convection electric field upstream of a discontinuity. Note that Figure 2 shows just one, simplified case in which an FB should form; the general criteria for FB formation remain an outstanding theoretical question, which we do not address further in this observational study. Upstream of the discontinuity, FBs grow back into the solar wind in time as more foreshock plasma is swept up at the discontinuity; the rising concentration of suprathermal plasma creates high temperatures resulting in a pressure imbalance, which the thermal solar wind plasma responds to by expanding. Due to this expansion, there are

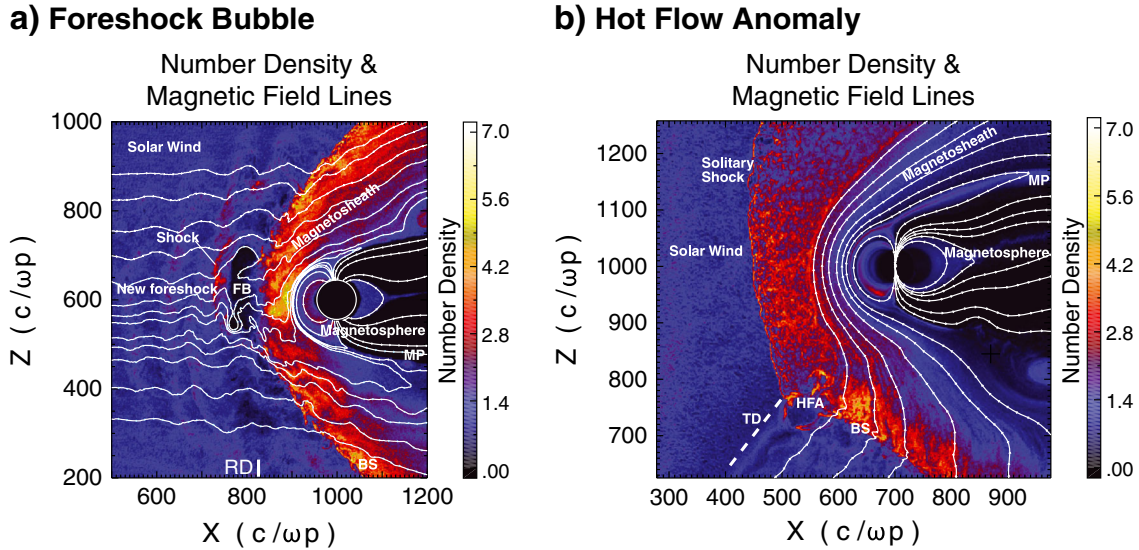


Figure 1. (a) 2.5-dimensional hybrid simulation results of a foreshock bubble [Omid *et al.*, 2010] showing the number density in color, normalized to the solar wind, and magnetic field lines. The X - and Z -axes are in units of the ion skin depth, where c is the speed of light and ω_p is the ion plasma frequency. The axes are in simulation coordinates; the origin is located beyond the lower left corner of the simulation box. The white circle around the Earth represents the simulation’s inner boundary, a dipole inside a perfectly conducting sphere. A rotational discontinuity (RD) in the IMF, indicated on the figure where the IMF changed from purely radial ($B_{\text{IMF}} \cdot [1, 0, 0]$ in XYZ) to having both an X and a Y component ($B_{\text{IMF}} \cdot [1, -0.5, 0]$ in XYZ), results in formation of a foreshock bubble (FB) exhibiting clear core and upstream shock features. (b) 2.5-dimensional hybrid simulation results of a hot flow anomaly [Omid and Sibeck, 2007] showing the number density in color, normalized to the solar wind, and magnetic field lines. The format is the same as shown in Figure 1a, but instead the HFA is related to a tangential discontinuity (TD) in the IMF.

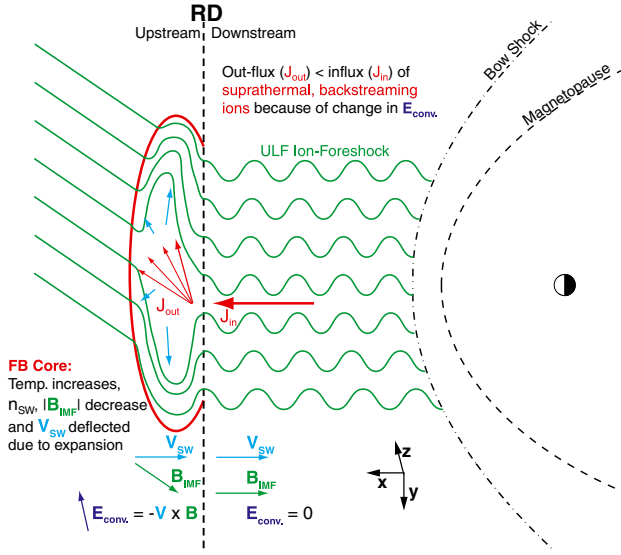


Figure 2. A schematic depicting an example formation scenario for a foreshock bubble. Here the IMF changes from purely radial to less so along a rotational discontinuity (RD). Here plasma velocities are shown with blue arrows, and magnetic field lines as green lines. In this example, an FB core forms due to the change in the convection electric field (E_{conv}) on the upstream side of the RD, resulting in the flux of suprathermal, backstreaming ions in the foreshock being lower than that on the downstream side ($J_{out} < J_{in}$). This occurs because E_{conv} produces an energy-dependent response on the backstreaming ions (depicted with different arrows on the upstream side). The concentration of these particles drives the local plasma temperature up rapidly just upstream of the RD, and in response, the thermal plasma expands, lowering the density and field strength (due to the frozen-in condition) and forming compression regions along the edges.

significant flow deflections, tenuous plasma, and low field strengths in the core, and a compression region of denser plasma and enhanced field strength (due to the frozen-in condition) develops around the outer edge. The upstream solar wind plasma impacting the growing FB must undergo pressure, velocity, density, and field transitions, resulting in the formation of a fast magnetosonic shock wave on the upstream edge of the compression region. This shock is also part of the FB structure (see Figure 1a), and the entire FB structure convects with the solar wind, i.e., at the solar wind speed and primarily in the negative X_{GSM} direction.

[6] Although FBs can form for a variety of IMF and rotational discontinuity orientations, they can only impact the magnetosphere when they form on the dayside, i.e., when the angle between the IMF downstream of the FB and solar wind velocity is small ($\leq \sim 45^\circ$). Perpendicular to the solar wind velocity direction, FBs scale with the width of the ion foreshock (i.e., tens of Earth radii, R_E , at Earth). Parallel to the velocity direction, FBs can grow to $\sim 10 R_E$ at Earth. A spacecraft observing an antisunward-moving FB in the foreshock would first observe the core, with its deflected flows, depressed density and field strength, and increased temperatures, and then the shock wave, exhibiting strong increases in density and field strength, behind it. From outside of the foreshock, a spacecraft should observe the core bounded by a compression region on the downstream side and the shock or a compression region on the upstream side (e.g., Figure 3b). The IMF discontinuity responsible for the event may become indistinguishable amongst the enhanced ULF waves in the original foreshock and core. For an example of this, see the results from hybrid simulations in Figure 3a. When FBs impact the magnetosphere, the density and magnetic field cavities in their cores result in sunward flows in the magnetosheath and magnetopause expansion, while the density and pressure enhancements associated with the subsequent shocks result in

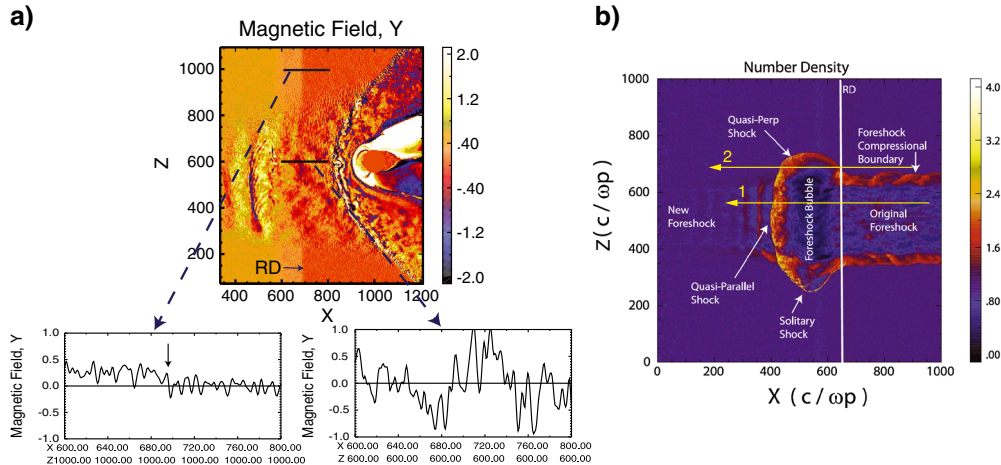


Figure 3. Two examples of caveats when observing foreshock bubbles: (a) Results from the same hybrid simulation as shown in Figure 1a but at an earlier time. B_z is shown in color with line plots corresponding to the two cuts (black lines, one in solar wind, one in foreshock) through the RD demonstrating how the ion foreshock can mask IMF discontinuities. (b) Results from local 2.5-dimensional hybrid simulations of a foreshock bubble demonstrating how a spacecraft observing the FB from initially within the foreshock (yellow arrow 1) would not observe any downstream compression region but just the FB core and upstream shock. However, a spacecraft observing an FB from the solar wind (yellow arrow 2) would observe a downstream compression region and an upstream shock around the FB core.

sudden compression of the magnetosphere. Effects of these changes should be observable in magnetic field measurements throughout the dayside magnetosphere. Because FBs involve two converging shocks (i.e., that of the FB and the bow shock), they should be efficient particle accelerators via Fermi and shock-drift acceleration processes.

[7] Another foreshock phenomenon, HFAs [e.g., *Schwartz et al.*, 1985; *Thomsen et al.*, 1986; *Paschmann et al.*, 1988; *Thomsen et al.*, 1988; *Omidi and Sibeck*, 2007; *Eastwood et al.*, 2008; *Zhang et al.*, 2010], exhibit many properties similar to FBs, including a relationship to IMF discontinuities, hot core temperatures, density and field depletions, deflected solar wind flows, shocks or compression regions bounding at least one side, and in situ observation times of ~ 1 to several minutes [*Facsko et al.*, 2008]. These similarities may explain why FBs have not been identified in previous observations. Current understanding suggests that HFAs form when suprathermal ions in the foreshock are guided and focused along an IMF discontinuity by the convection electric field on one or both sides of the discontinuity. When this occurs, suprathermal ions are focused into the discontinuity causing the temperature and thermal pressure to be greatly enhanced at a finite region around the intersection between the discontinuity and the bow shock. This drives thermal plasma out of this region to maintain pressure balance, resulting in depressed field strengths and densities. The ejected plasma piles up at the edges of HFAs producing compression regions that may form into shocks depending on the HFA geometry and motion with respect to the incident solar wind. Figure 1b shows hybrid simulation results [*Omidi and Sibeck*, 2007] of a fully developed HFA formed due to a tangential discontinuity interacting with the bow shock. Note that the most intense HFA core and compression region features are near the intersection point of the discontinuity and the bow shock.

[8] Despite these similarities, HFAs and FBs form independently and have distinctly different structures. HFAs are transient features that form and move along the bow shock at the intersection curve between the bow shock and a discontinuity in the IMF. Thus, their motions (and observed durations) are fully dependent on the orientation of the discontinuity with respect to the local bow shock. Based on simulations [*Schwartz*, 1995; *Omidi and Sibeck*, 2007], HFAs along Earth's bow shock should only be on the order of a few R_E in size both along the bow shock (normal to the discontinuity) and normal to it, but they are elongated along the discontinuity intersection line with the bow shock. Considering the similarities between HFAs and FBs observed in situ, care must be taken when using multispacecraft observations to distinguish between the two. Key differences, which can be used as identification criteria, are:

[9] (1) HFA formation requires that an IMF discontinuity be intersecting to the bow shock but FB formation does not;

[10] (2) HFAs form upstream (if the IMF changes from quasi-perpendicular downstream to quasi-parallel upstream), around (if the discontinuity maintains quasi-parallel conditions on both sides) or downstream (if the IMF changes from quasi-parallel downstream to quasi-perpendicular upstream) of rotational or tangential discontinuities [*Omidi and Sibeck*, 2007; N. Omidi, private communication, 2012]; FBs should only form upstream of some rotational discontinuities;

[11] (3) FBs can be $10 R_E$ or more in size and can form far upstream of the bow shock. In contrast, HFAs are only a few R_E in width normal to the discontinuity, form at the bow shock, and their features diminish rapidly within a few R_E away from the bow shock;

[12] (4) FBs convect with the solar wind, but HFAs move along the bow shock with the discontinuity intersection;

[13] (5) HFAs require that the electric field on one or both sides of the discontinuity be pointed back into it, whereas FBs do not;

[14] (6) Except in the extreme case of a reflected-to-incident ion density ratio of more than $\sim 65\%$ [*Thomsen et al.*, 1988], HFAs are bounded on both sides by compression regions, which may or may not form into shocks, but FBs observed from within the foreshock should only be bounded on the upstream side by a compression region or shock;

[15] (7) The normal direction of the shock or compression region that forms on the upstream side of an FB should have a very strong, and likely dominant, GSM-X component for most spacecraft trajectories through it, whereas the normal direction of the shock/compression on the upstream side of an HFA can exhibit a range of orientations because the HFA forms approximately parallel to the IMF discontinuity at the bow shock, resulting in compression regions with normal directions that are initially perpendicular to this (though these likely change in time as the HFA evolves and interacts with the solar wind) [see also *Paschmann et al.*, 1988].

3. Data and Methods

[16] For this study, we employed observations from NASA's THEMIS mission [*Angelopoulos et al.*, 2008], consisting of five identically instrumented spacecraft that were launched in early 2007 and an extensive network of ground-based observatories. We examined data from the dayside-2008 phase of the mission (i.e., July–October 2008), when THEMIS-B (TH-B) and -C were regularly upstream of Earth's bow shock at their respective apogees. For this study, we used THEMIS solid state telescope (SST) energetic ion data, electrostatic analyzer (ESA) plasma data [*McFadden et al.*, 2008]), and fluxgate magnetometer data [*Auster et al.*, 2008]). For the SST ion data, sunlight contamination was removed, and we used the latest data available, which have been characterized in Geant4 and intercalibrated for look direction, ensuring quality angular distributions.

[17] Figure 4 shows the spacecraft locations in GSM coordinates at the times of each event examined in this study. Colors represent the two spacecraft, while different symbols are for each event examined here, as listed in the legend. For all events, TH-B (blue symbols) was upstream of the bow shock on the dayside, near apogee, at radial distances between around 25 and 30 R_E ; TH-C (red symbols) was in the same local time sectors for each event, though at $\sim 18 R_E$, it was closer to the average bow shock location [*Fairfield*, 1971]. For each example case shown here, we show simultaneous TH-B and -C data from 8 min periods around each event. This allows for direct comparison between the upstream TH-B observations and those at TH-C, which captured the fully formed events. Note that for all of the events, the ion and electron densities from ESA reveal good agreement between the species, indicating that the instruments captured the narrow solar wind beam. However, the ESA instruments were most

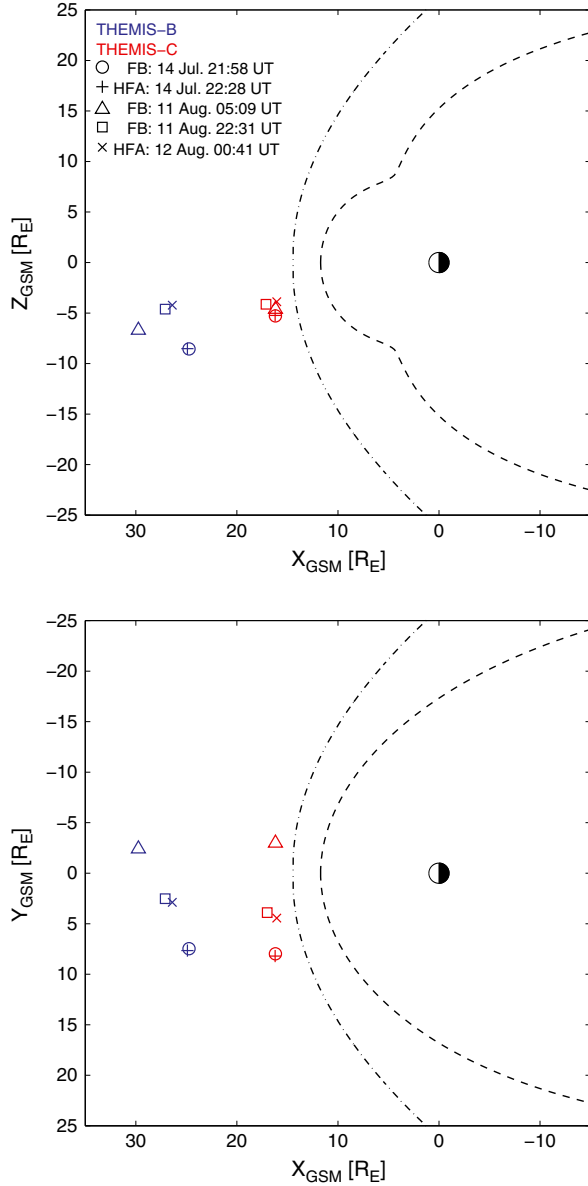


Figure 4. Spacecraft locations during each of the example events: the top plot shows THEMIS-B (blue) and -C (red) locations in the XZ_{GSM} plane, while the bottom plot shows them in the XY_{GSM} plane. Different symbols correspond to different events, as indicated in the legend. Bow shock (BS) and magnetopause (MP) models [Fairfield, 1971; Lin et al., 2010] are shown with the dashed lines.

often in magnetospheric mode and thus, do not capture the absolute value of the cold, pristine solar wind ion temperature (though variations are often well captured) [McFadden et al., 2008]. To account for this, we compared the THEMIS temperatures, calculated from ESA on board plasma moments in the solar wind, to those measured upstream by various spacecraft comprising the OMNI data set. For each event presented in the following sections, we discuss key features in the TH-B and -C observations followed by detailed analysis, in which we step through the seven identification criteria for HFAs and FBs introduced in section 2 to determine which of these two phenomena best describe the events examined here.

[18] Minimum variance analysis (MVA) [e.g., Sonnerup and Scheible, 1998] and coplanarity analysis [e.g., Schwartz, 1998] are used here to determine the orientation of the various IMF discontinuities in this study. MVA relies on the divergence of B being zero, such that across a discontinuity boundary, the component of the magnetic field normal to the boundary must remain constant. Thus, MVA uses vector analysis of a number of samples through a discontinuity to determine the direction (i.e., unit vector) along which the variance in the field vectors is minimized (ideally, it should be equal to zero). Standard tests for the quality of an MVA fit include the minimum-to-intermediate eigenvalue ratio test ($\lambda_3/\lambda_2 < 0.1$ implies a reliable fit) and a sensitivity test verifying that the calculated normal doesn't vary significantly for small changes to the range of vectors used as input. However, MVA fails for pure MHD shocks [Schwartz, 1998], and for these cases, coplanarity can be employed. The coplanarity theorem, based on the Rankine-Hugoniot jump conditions across shocks, states that the magnetic field on either side of a shock and the normal direction to the discontinuity all lie in the same plane. This can be used to establish a system of equations for vectors that lie either in the coplanarity plane or perpendicular to it, and from this system, the normal direction to the discontinuity can be calculated [for more details see Schwartz, 1998]. Another technique that can be used for determining the normal directions to tangential discontinuities is the cross-product analysis [Schwartz, 1998]; in this method, the normal direction is simply estimated as the unit vector of the cross-product between the upstream and downstream magnetic field vectors. A major caveat of coplanarity and cross-product analyses is the difficulty in establishing the true field direction immediately upstream and downstream of the discontinuity plane, because observations are often affected by waves, turbulence, localized ripples on the discontinuity “surface”, or other IMF rotations nearby. We have analyzed each of the IMF discontinuities in question using the MVA and cross-product methods and compared the results. Distinguishing between rotational and tangential discontinuities is complex (i.e., most rotations in the IMF fall somewhere between these ideal theoretical cases) and is not critical to the results of this study, so we simply checked the plasma and field observations for classic signature of each type of discontinuity and also calculated the normal component of the magnetic field through the discontinuities, which should be finite or zero for rotational or tangential discontinuities, respectively [e.g., Berchem and Russell, 1982]. Also, because compressional discontinuities are rarely pure MHD shocks, we have analyzed each of the suspected shocks (or strong compressions) using the MVA and coplanarity methods.

[19] From the discontinuity orientations we can establish if the discontinuity plane was connected to the bow shock at the time it was observed at each spacecraft using the Fairfield [1971] bow shock model. Because of the three-dimensional geometry of the system, including spacecraft separations, the time difference between TH-B and -C observing the same discontinuity is estimated by dividing the distance between the spacecraft in the normal direction to the discontinuity by the component of the solar wind velocity normal to the discontinuity. This is also what is used to estimate the size of HFA-like events in this work, because HFAs form and move along the bow shock as a

discontinuity passes over that boundary. For FBs, which pass by a spacecraft with the solar wind velocity, their size in the GSM-X direction is estimated by multiplying the unperturbed solar wind speed by the length of time the FB is observed by the spacecraft. Finally, the electric field is calculated on both sides of each discontinuity using the observed ion velocity and magnetic field vectors, and the orientation of the discontinuity is used again to determine if the E -field is pointed back into the discontinuity on the upstream and/or downstream sides.

4. Examples From Bastille Day 2008

4.1. Foreshock Bubble Example 1

4.1.1. Observations

[20] Figure 5 shows the TH-B and -C observations from the period of interest for the first example event. Here we focus on the features observed by TH-B centered around ~21:57 UT and TH-C centered around ~21:58 UT (gray shaded regions in Figure 5). Between 21:53 and 21:57 UT, TH-B and -C observed additional plasma variations. These are of interest but are not directly relevant to the main aspect of this case study, and they are briefly discussed in the Discussion section. During this period, the solar wind speed was steady and above average, at ~620 km/s. Just after 21:56 UT, TH-B observed a rotational discontinuity in the IMF, indicated by the yellow shaded region in Figure 5. We consider this a rotational discontinuity because it was not associated with any discontinuous features in the plasma density, thermal pressure (not shown), magnetic field strength, or velocity magnitude, and the normal component of the magnetic field on both sides was finite (discussed in the next section). Just prior to this, the plasma velocity vector changed direction, exhibiting a briefly weakened V_X and negative enhancement in V_Y associated with a previous IMF rotation. Following the latter rotational discontinuity, from 21:56:06 to 21:57:36 UT, TH-B observed a depression in total field strength and density (to ~1 nT and ~0.3 cm⁻³, respectively) and an enhancement in ion (up to ~500 eV) and electron (up to ~30 eV; not shown) temperatures, indicated by the gray shaded region in Figure 5.

[21] THEMIS-C observed the same (see analysis in section 4.1.2 below) IMF rotational discontinuity around one minute after TH-B. Following the discontinuity, TH-C observed slow decreases in field strength and density and a slow increase in electron temperature. Then starting at ~21:57:35 UT, the magnetic field strength and the ion and electron densities dropped suddenly to ~1 nT and ~0.1 cm⁻³, respectively, in association with rapid increases in both ion (up to ~2000 eV) and electron (up to ~200 eV; not shown) temperatures. Note that because the solar wind ion beam is dispersed in the cores of the features shown here, the ion temperatures calculated from the on board moments are more likely representative of the actual temperature. Subsequently, the local plasma velocity reversed direction, with a small positive V_X component indicating sunward flows from 21:57:48–21:58:06 UT. The Y_{GSM} and Z_{GSM} components of the velocity were both enhanced through this encounter, with strong positive V_Y and negative V_Z both greater than 200 km/s, as expected for magnetosheath deflections based on the spacecraft location (Figure 4). The solar wind ion beam was heated, i.e., spread over a broad

range of energies, and there was a several orders of magnitude enhancement in the energetic ($E > 1$ keV) electron flux. This was clearly not just a bow shock crossing, because both the field strength and density diminished. This encounter culminated in well-formed shocks observed between 21:58:12 and 21:58:20 UT. The shocked plasma exhibited a very strong magnetic field strength (peaking at ~28 nT), density (> 10 cm⁻³), and greatly enhanced total pressure ($> 10\times$ the ambient solar wind pressure).

4.1.2. Analysis

[22] Decreases in field strength and ion density associated with increases in ion temperature characterize the cores of both HFAs and FBs in the ion foreshock, and both TH-B and -C observed such signatures associated with this event. Observed by TH-C alone with no awareness of FBs, the features in question (i.e., gray shaded region in Figure 5) could have been interpreted as those of an HFA, because central density and field strength dropouts, temperature enhancements, deflected solar wind flows, and shocks on either one or both boundaries all characterize observations of HFAs near planetary bow shocks. Both FBs and HFAs are associated with IMF discontinuities: for this case, an FB would form upstream of the IMF discontinuity while an HFA core would form at the downstream side of the discontinuity (criterion 2). For this first event, TH-B and TH-C both observed the same discontinuity and the event itself upstream of it, consistent with criterion 2 for FBs. This discontinuity rotates the IMF by ~100 degrees, which suffices to generate an FB [Omid et al., 2010]. Both ACE and Wind (data available on CDAWeb but not shown here), which were $> 225 R_E$ upstream of the Earth and separated by ~106 R_E , observed multiple IMF rotations between 21:00 and 21:30 UT. Accounting for the ~35–40 min transit time between these spacecraft and TH-C, it is possible that one of these was the same observed by the THEMIS spacecraft and responsible for this transient foreshock event. However, Wind and ACE observed strikingly different IMF features, making any timing analysis using these spacecraft problematic.

[23] Minimum variance analysis on the IMF rotation at TH-B between 21:55:55 and 21:56:15 UT reveals a good fit ($\lambda_3/\lambda_2 < 0.03$) and a normal direction of [0.58, -0.60, -0.56] in GSM. Cross-product analysis using upstream and downstream TH-B field observations revealed a normal direction of [0.47, -0.66, 0.59]. MVA with TH-C fields between 21:57:04 and 21:57:09 UT confirmed that it is the same rotation, revealing a well-fit ($\lambda_3/\lambda_2 = 0.10$) normal direction of [0.58, -0.60, -0.56] in GSM (cross-product analysis revealed a normal direction of [0.25, -0.67, 0.70], also generally consistent with the cross-product normal from the TH-B discontinuity). We proceed using the MVA normal direction because of the consistent results and good fits from TH-B and -C. The normal component of the magnetic field remained finite (i.e., it remained greater than 2 nT) throughout the discontinuity, so it was most likely a rotational discontinuity. Calculating electric fields upstream and downstream of the discontinuity at both spacecraft revealed that the electric field upstream was pointed back into the discontinuity. Thus, we cannot rule out an HFA based on criterion 5. The normal direction also revealed that the discontinuity was already connected to the bow shock prior to the observations by TH-C and TH-B (criterion 1 for HFAs). If this event was an HFA that formed about the

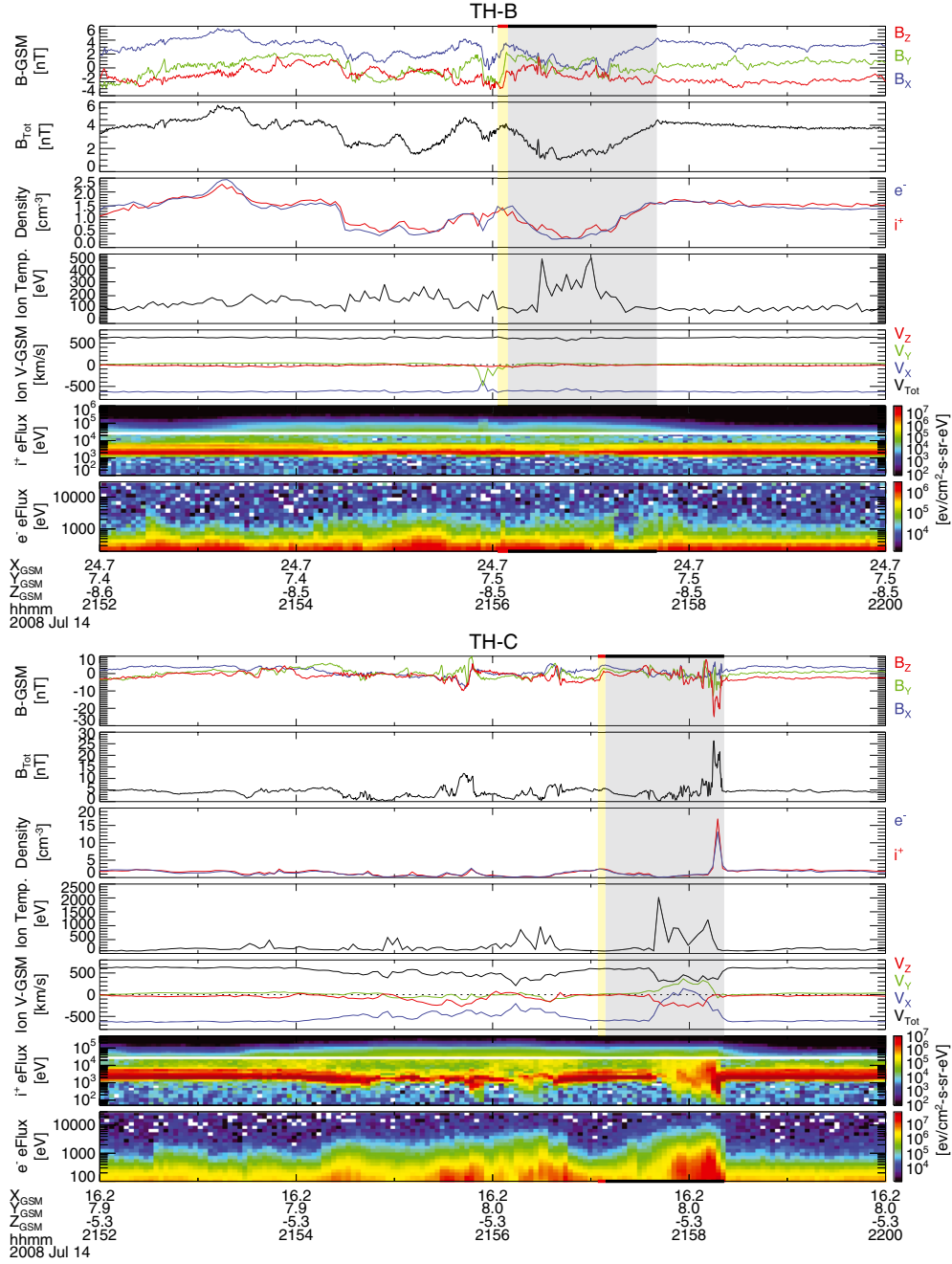


Figure 5. TH-B (top) and TH-C (bottom) observations during the first FB example period: 21:52–22:00 UT on 14 July 2008. For the plots from each spacecraft, the following quantities are plotted from top to bottom: B-GSM: the magnetic field components in GSM (XYZ in blue, green, red); B_{Tot} : the total field strength (black); Density: the ion (red) and electron (blue) density; Ion Temp.: the ion temperature (note the ion temperature in the pristine solar wind from OMNI was ~ 15 eV during this period); Ion V-GSM: the ion velocity components in GSM (XYZ in blue, green, red) and the speed (black); i^+ and e^- eFlux: the high and low-energy ion (i^+ , as measured by two different instruments, SST and ESA) and ESA electron (e^-) flux spectrograms. Note that the scales are different between TH-B and -C plots of the same quantities. The yellow shaded regions indicate discontinuities of interest and the gray shaded regions indicate the events themselves.

examined discontinuity or some different discontinuity (that may be masked by wave activity in the event's core), we would expect from criterion 7 that the shock that forms on the upstream edge would have a normal direction that is oblique to the solar wind velocity and quasi-parallel to

that of the IMF discontinuity normal. On the other hand, an FB shock should have a normal direction that has a strong or dominant X -component. Using the upstream shock crossing in high-resolution TH-C magnetic fields to calculate average upstream and downstream vectors from

21:58:20.95–21:58:21.0 (upstream) and 21:58:16.6–21:58:18.6 (downstream), the normal direction to the shock was calculated using magnetic coplanarity. This revealed a shock normal of $[0.95, 0.24, -0.16]$ in GSM coordinates, consistent with what is expected for an FB. Using MVA during the same downstream-to-upstream period, a normal direction of $[0.59, 0.34, -0.72]$ was calculated, but the quality test showed this was a very poor fit ($\lambda_3/\lambda_2 = 0.80$). Other attempts at MVA using different periods around and within this shock also proved inconsistent and inaccurate.

[24] Hot flow anomalies should be bounded on both sides by compression regions, which result from a pressure balance with the hot core (see example HFA in Figure 1b); however, a spacecraft observing an FB from within the foreshock should not observe a compression region on the downstream side (e.g., Figure 3b). TH-C observed no downstream compression region associated with the event's core features. The reflected to incident density ratio was less than 0.1 based on TH-C densities calculated in the foreshock at 21:57 UT for the solar wind beam (using $E = 1\text{--}3$ keV from ESA, $n_{\text{incident}} = 1.8 \text{ cm}^{-3}$) and the backstreaming ions (using $E = 3\text{--}300$ keV from ESA and SST, $n_{\text{reflected}} = 0.1 \text{ cm}^{-3}$), which means that the downstream side of an HFA would have formed a compression region [Thomsen *et al.*, 1988]. Thus, this event is inconsistent with criterion 6 concerning compression regions bounding HFAs.

[25] Lastly, using the timing of the discontinuity (i.e., onset of the core features) observed at TH-B and -C, a timing analysis revealed a transit time of only ~ 1 min between the two spacecraft. Based on the total observation times, the size of the event in the X_{GSM} direction (assuming motion with the solar wind, like an FB) would have been $\sim 9.2 R_E$ at TH-B and $\sim 7.3 R_E$ at TH-C. However, assuming HFA-like motion along the bow shock using the normal direction calculated above, the event would have been $\sim 5.4 R_E$ at TH-B and $\sim 4.3 R_E$ at TH-C in the normal direction. This is not as would be expected of an HFA, which should grow in time in the normal direction and be much larger closer to the bow shock. Furthermore, moving with the discontinuity plane along the bow shock, it would have taken ~ 2 min to travel between TH-B and -C. These are inconsistent with an HFA, considering criteria 3 and 4. Interestingly, the discontinuity and event were moving faster than they should in the ~ 620 km/s solar wind (at 620 km/s, the solar wind should take 90 s to travel between TH-B and -C), indicating that as the event evolves, it may be distorting the planarity of the discontinuity and/or also pushing the plasma ahead of it. The discrepancy in timing may also result from complex spatial and temporal evolution of the plasma resulting from the event itself or its interaction with the bow shock, which should have occurred near the time when TH-C observed it. Such complex evolution or interactions may also explain the difference in the size of the event observed by each spacecraft.

[26] Summarizing, this event: (1) was observed more than $10 R_E$ upstream of the bow shock, (2) was convected by the solar wind, (3) was between 7 and $9 R_E$ in size in the X_{GSM} direction, and (4) exhibited no compression region on the downstream side and a well-formed shock on the upstream side that had a normal direction nearly parallel to X_{GSM} . Additionally, there was an IMF

discontinuity downstream of the event that rotates sufficiently to generate an FB. Each of these features is inconsistent with the expected results for HFAs and consistent with those for FBs.

4.2. Hot Flow Anomaly Example 1

4.2.1. Observations

[27] It is important to quantify the differences between FBs and HFAs considering their numerous similarities in single-spacecraft time series data and that FB observations may have been misinterpreted as HFAs in the past. Figure 6 shows TH-B solar wind observations and TH-C observations of an HFA on the same day as the observations of the first example FB (14 July 2008). These two events are separated by only ~ 30 min in time, during which the formation conditions in the solar wind and foreshock are very similar as can be seen by comparing TH-B observations in Figures 5 and 6. Figure 6 shows upstream observations by TH-B during the period around which TH-C observed an HFA. As in the previous event, the solar wind speed was steady and above average, at ~ 600 km/s. There were two IMF rotations during this period: the first between 22:27:10 and 22:27:30 UT and the second around 22:28:33 UT. At TH-B, suprathermal ions and correlated magnetic field strength and density variations, both evidence of the ion foreshock, are evident around the time of the first discontinuity but not during the second. Note that there were no significant temperature or velocity variations associated with either of these, though there were slight enhancements in the suprathermal electron population.

[28] Observations closer to the bow shock measured by TH-C are shown in the bottom of Figure 6, which reveal the two discontinuities in the IMF observed upstream previously by TH-B. These IMF rotations are seen at TH-C between 22:28:10 and 22:28:30 UT and around 22:29:10 UT, respectively. Around the first rotation appeared a cavity-like structure with enhanced regions on either side of a core with depressed magnetic field strength and density. Corresponding to the low field strength and tenuous core region observed at around 22:28:30 UT was a sharp enhancement in ion temperature (up to ~ 1200 eV), ion flow deflections (V_X slows corresponding to an increase in $+V_Y$ and $-V_Z$), and a dispersion of the solar wind ion-beam.

[29] The second IMF discontinuity, mentioned above, was also observed at TH-C around 22:29:10 UT. Another cavity in the field strength and density was observed associated with this discontinuity, and there was a compression region on the downstream side. However, there was no significant temperature increase, flow deflection, or dispersed ions associated with the discontinuity. For these reasons, we do not analyze this second discontinuity here.

4.2.2. Analysis

[30] We calculated an MVA for the discontinuity associated with this event to determine the discontinuity plane's normal direction and propagation time between the two spacecraft. Using the rotations observed at TH-B between 22:27:26 and 22:27:29 UT, the analysis revealed a good fit ($\lambda_3/\lambda_2 = 0.09$) with a normal direction of $[0.64, -0.05, 0.77]$ in GSM. Cross-product analysis revealed a normal direction of $[0.71, 0.49, 0.51]$ in GSM using average upstream and downstream fields from 22:27:35–22:27:40 UT and 22:27:22–22:27:24 UT, respectively. The

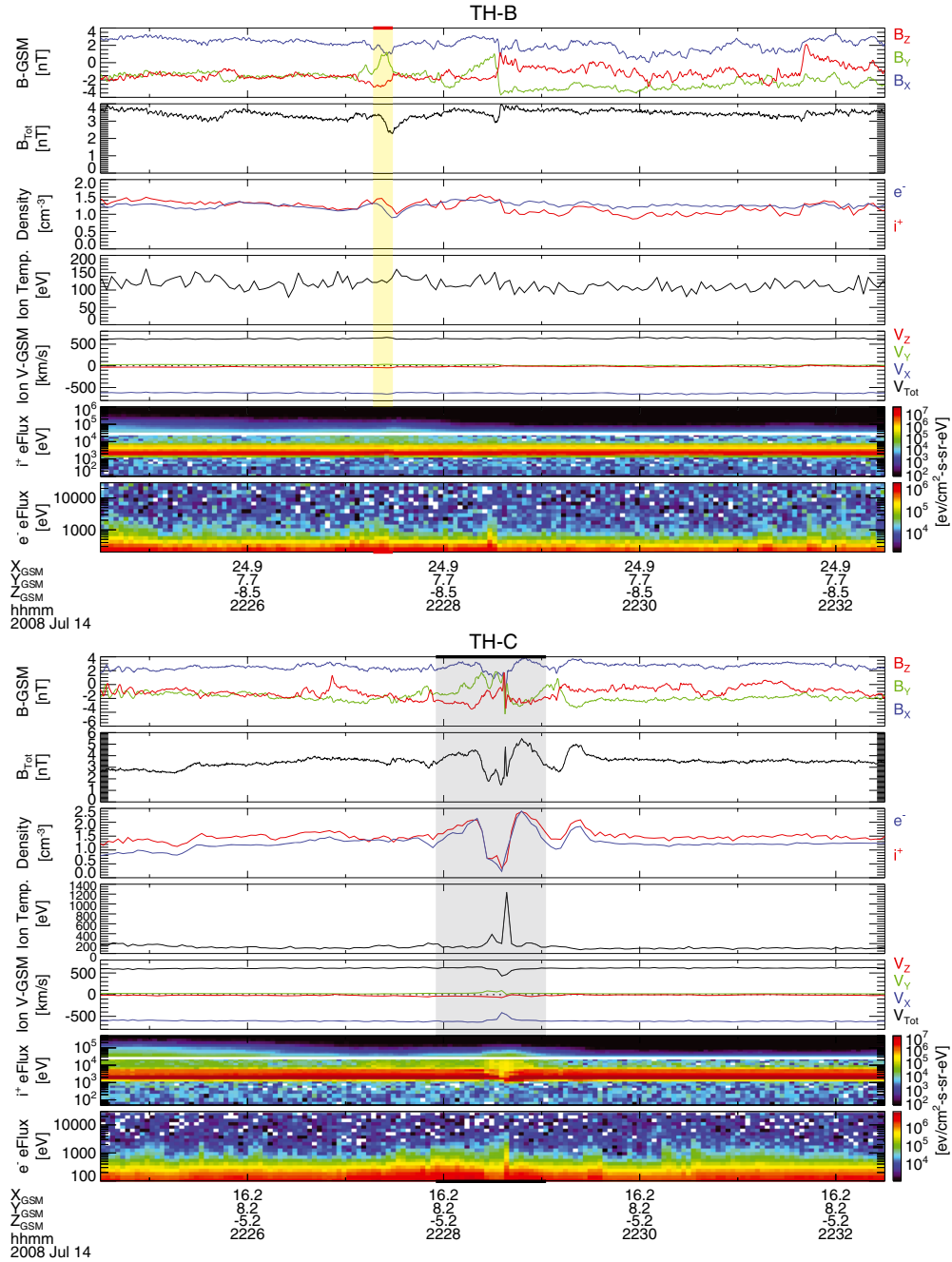


Figure 6. TH-B (top) and TH-C (bottom) observations during the first HFA example period: 22:24:30–22:32:30 UT on 14 July 2008. The format is the same as described in Figure 5. The ion temperature in the pristine solar wind from OMNI was ~ 15 eV during this period.

disagreement between the two vectors may be explained by an inaccurate downstream period for cross-product analysis due to the presence of multiple rotations in the field in close succession; for this reason, we proceeded with the MVA orientation, because it revealed a good fit. The normal component of the magnetic field (B_N) was very small on either side of the discontinuity (i.e., < 1 nT). Through the discontinuity, B_N passed through zero and changed sign, so this was possibly a tangential discontinuity. With the MVA orientation, it should have taken ~ 1 min to travel between the two spacecraft if moving along the discontinuity normal direction (i.e., as an HFA would along the bow shock). Based on this

normal direction, the discontinuity should have already intersected the bow shock before it was observed at both TH-B and -C (criterion 1 for HFAs). From the convection electric fields calculated upstream and downstream of the discontinuity at TH-B, the upstream E -field pointed back into the discontinuity, satisfying that important formation criterion (criterion 5) for HFAs. The propagation time between the two spacecraft is consistent with that observed (~ 70 seconds), again considering distortion due to the event formation and evolution. The normal direction was used to estimate the size of the feature observed at TH-C; assuming it was moving along the bow shock, the event is $\sim 4.9 R_E$ in

width in the discontinuity normal direction, consistent with criterion 3 for HFAs. We also performed an MVA on the upstream compression region for this event between 22:28:50 and 22:29:12 UT, and it revealed a good fit ($\lambda_3/\lambda_2 = 0.10$) with normal direction of $[0.50, -0.86, 0.05]$ in GSM. This normal is not primarily in the GSM-X direction, which is inconsistent with criterion 7 for FBs. Again, we could not find a consistent match with coplanarity, likely due to complications from additional kinetic effects on either side of the compression region, though we have confidence in the MVA result due to a good fit and consistent result when the input period is slightly perturbed.

[31] This event exhibited a magnetic field strength and plasma density cavity flanked on both sides by enhanced field strength and density regions, a hot central core, deflected plasma flow, and the presence of suprathermal ions and electrons; these are all classic features of HFAs. The required formation criteria of an electric field pointed back into the discontinuity was satisfied, and the orientation of the compression region on the upstream side was consistent with this feature forming along the bow shock. Assuming motion along the bow shock, the estimated size at TH-C is consistent with what is expected for fully developed HFAs based on hybrid simulations. This event formed centered around the responsible discontinuity, not upstream of it (criterion 2 for HFAs). These all indicate that this event was an HFA. Despite the discontinuity already being in contact with the bow shock, TH-B observed no HFA-like features associated with the discontinuity, which is expected based on the scale and nature of HFAs in hybrid simulations. Interestingly, this HFA did not significantly heat electrons above those in the foreshock.

5. Additional Cases From 11 to 12 August 2008

[32] We now examine three more examples of transient foreshock phenomena to establish that the observations classified as an FB above are not unique. Like the Bastille Day examples, these examples are all from the same 24 h period, and the formation conditions in the solar wind and foreshock were similar for each event.

5.1. Foreshock Bubble Example 2

5.1.1. Observations

[33] Figure 7 shows TH-B and -C observations from an 8 min period on 11 August 2008. Around 05:04:24 UT, TH-B observed a $\sim 79^\circ$ rotation in the IMF, in which the Y -component changed from negative to positive with slight changes in the X - and Z -components. At the time of the discontinuity, TH-B observed a slight drop in field strength and plasma density and a ~ 100 km/s enhancement in V_Y . The solar wind speed during this period was steady at ~ 600 km/s. Between $\sim 05:06:00$ and 05:07:30 UT, TH-C observed a slight enhancement in the magnetic field strength and density and the presence of suprathermal ions. This is consistent with the spacecraft passing through the foreshock compressional boundary (FCB) into the ion foreshock, most likely in response to the IMF rotation. After passing through the compressional boundary, TH-C observed the transient foreshock event characterized by: a drastic decrease in field strength (< 1 nT) and density (< 1 cm $^{-3}$), an increase in electron and ion temperatures (ion temperature up to ~ 2300 eV; electron temperature up to ~ 240 eV, not shown),

highly-deflected and slowed flows ($V_X \sim 0$ km/s), and an enhancement of energetic electrons between $\sim 05:07:30$ and 05:09:00 UT. Immediately following this, between 05:09:00 and 05:09:10 UT, TH-C observed a strong enhancement of the magnetic field (up to ~ 15 nT from a baseline of ~ 3 nT) and density (up to ~ 6 cm $^{-3}$ from a baseline of ~ 1 cm $^{-3}$). Corresponding to these enhancements, the temperature and velocity returned to approximately pre-event levels, and based on the ion energy-flux distributions, the spacecraft returned to typical foreshock plasma. These sudden enhancements in field strength and density are consistent with the spacecraft passing through a shock-like structure. However, like the first example event, this period was not a bow shock crossing because the plasma and field observations are inconsistent with those in the sheath. Around 05:10:15 UT, TH-C observed what appears to be a forming HFA, which we do not analyze here.

5.1.2. Analysis

[34] Performing MVA on the discontinuity observed at TH-B between 05:03:55 and 05:04:51 UT revealed a reasonable fit ($\lambda_3/\lambda_2 = 0.12$) and normal direction of $[0.50, -0.72, -0.47]$ in GSM coordinates. Cross-product analysis again failed to reveal a consistent normal direction ($[0.33, -0.19, -0.92]$), possibly due to wave activity on both sides of the discontinuity or complexities due to multiple IMF rotations in close succession. With the MVA orientation, B_N passed through zero and changed sign through the discontinuity, so this was possibly a tangential discontinuity. The discontinuity should have taken ~ 2.5 min to be observed later at TH-C, which is approximately consistent with the turning of the foreshock evident from the observation of the foreshock compressional boundary by TH-C around 05:07 UT. When TH-B observed the discontinuity, it was already connected to the bow shock, and an analysis of the electric fields on either side revealed that they were indeed pointed back into the discontinuity on both sides. The size of the event at TH-C was either $5.2 R_E$ in the normal direction of the discontinuity (HFA-like motion, using the discontinuity geometry) or $10.1 R_E$ in the X_{GSM} direction (FB-like motion, with the solar wind velocity). Not considering the foreshock compressional boundary as part of the event, there was no compression region on the downstream side, and the reflected-to-incident density ratio observed by TH-C at $\sim 05:07:30$ UT was ~ 0.1 . This means that an HFA should have formed a downstream compression region (criterion 6). Finally, coplanarity analysis on the shock-like structure at the upstream edge of the event revealed a normal direction of $[0.91, -0.37, -0.16]$ in GSM, indicating an FB-like geometry (criterion 7 for FBs). With only 3 s resolution data available, it was not possible to get a good, consistent fit on the discontinuity using MVA.

[35] Summarizing, this event was most likely related to the IMF discontinuity observed by TH-B at $\sim 05:04:24$ UT. The conditions were consistent with those for an HFA because the IMF was connected to the bow shock at the time of the discontinuity passage by the spacecraft (criterion 1) and the convection electric fields on either side pointed back into the discontinuity (criterion 5). However, timing analysis and TH-C data showed that the discontinuity was downstream of the event, with the event itself following after it (criterion 2 for FBs). There was no compression region on the downstream side of the event, though the reflected-to-incident density ratio showed that an HFA should have formed a compression region on both sides for these conditions

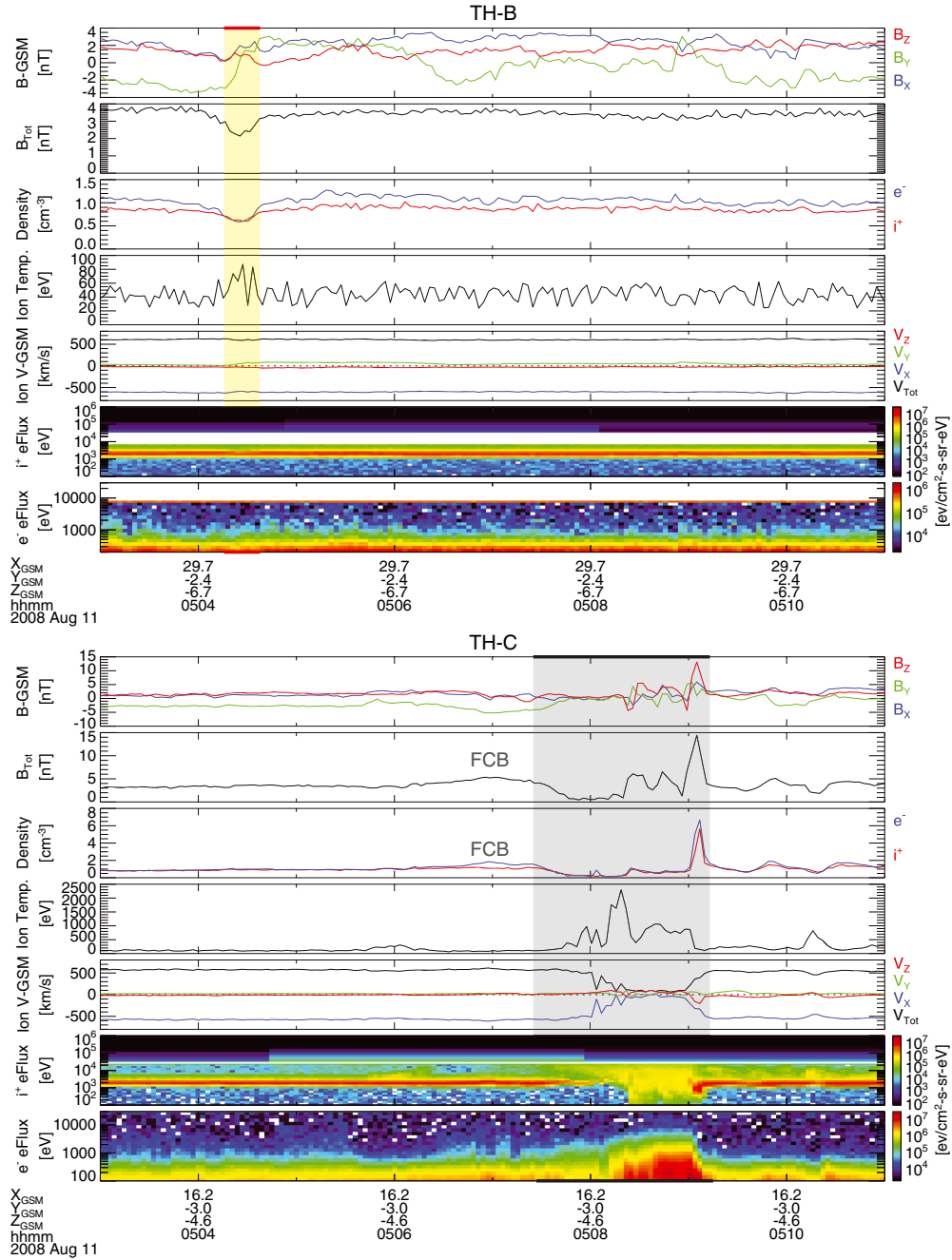


Figure 7. TH-B (top) and TH-C (bottom) observations during the second FB example period: 05:03–05:11 UT on 11 August 2008. The format is the same as described in Figure 5. Note that the TH-B ESA was in solar wind mode, and the ion temperature in the pristine solar wind from OMNI was ~ 17 eV during this period.

(criterion 6 against HFAs). The shock on the upstream side revealed a normal direction with a dominant X -component (criterion 7 for FBs). Thus, the characteristics of this event were most consistent with those of a foreshock bubble, and indeed, assuming motion with the solar wind, this event was the correct size for an FB (criteria 3 and 4), at $\sim 10 R_E$ parallel to the X_{GSM} direction.

5.2. Hot Flow Anomaly Example 2

5.2.1. Observations

[36] THEMIS-C observed the passage of a transient foreshock event in the early hours of 12 August 2008. Like the

previous examples, TH-B was further upstream than TH-C, which was closer to the bow shock (Figure 4), and the solar wind was steady with no large density or velocity perturbations and speed of ~ 600 km/s. Upstream, TH-B observed two rotational discontinuities in the IMF: the first starting just before 00:38:00 UT and the second at around 00:38:50 UT. These rotations were apparently some embedded structure within the IMF, because the field directions at the beginning and end of the 8 min period shown in Figure 8 are very similar. Nevertheless, these rotations were also observed closer to the bow shock by TH-C between around 00:40:10 and 00:41:20 UT. Associated with these changes

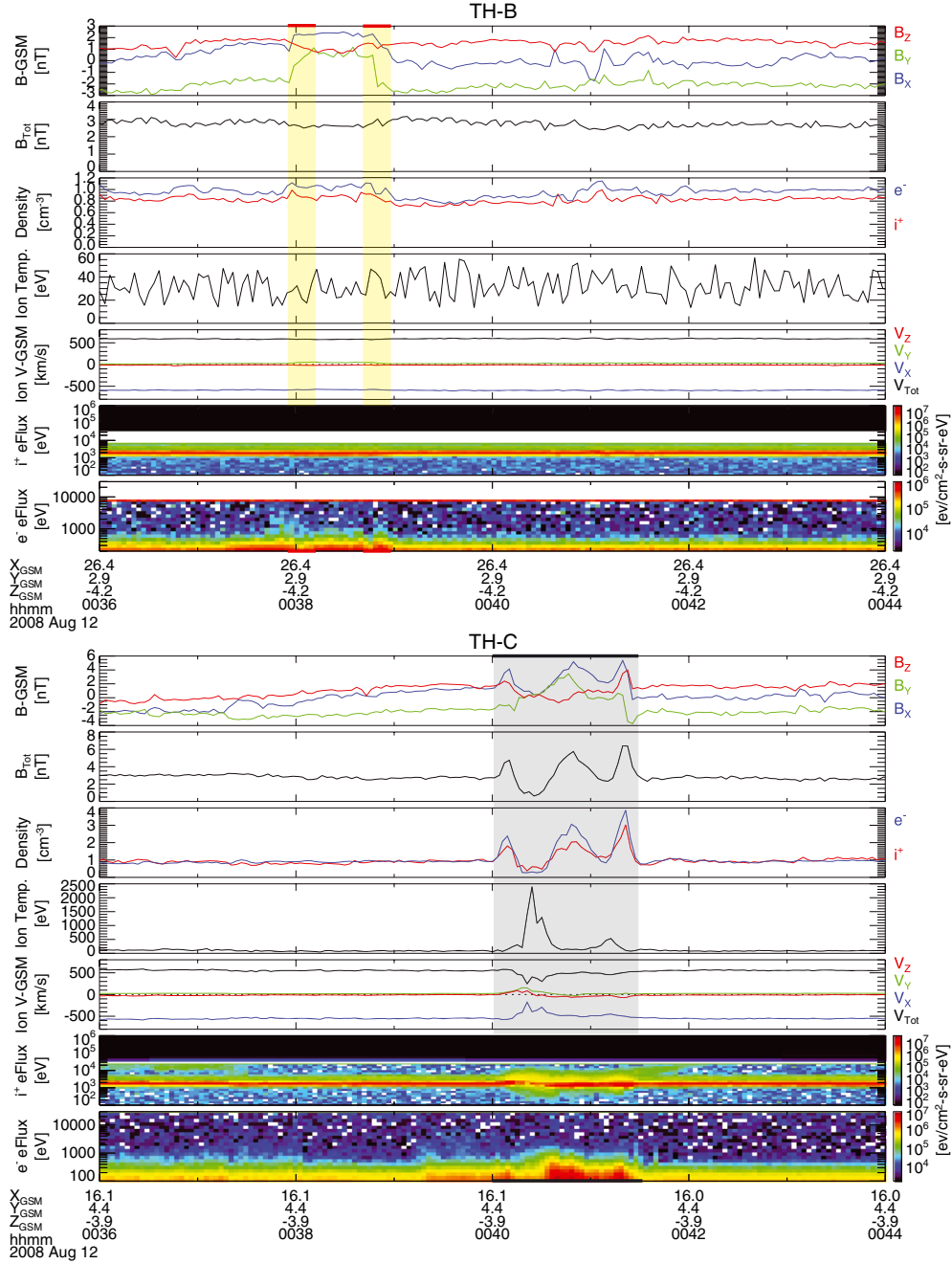


Figure 8. TH-B (top) and TH-C (bottom) observations during the second HFA example period: 00:36–00:44 UT on 12 August 2008. The format is the same as described in Figure 5. Note that the TH-B ESA was in solar wind mode, and the ion temperature in the pristine solar wind from OMNI was ~ 10 eV during this period.

in the IMF orientation, TH-C observed correlated variations in the magnetic field strength and plasma density, an enhancement of ion and electron temperature (ions up to ~ 2400 eV; electrons up to ~ 23 eV, not shown), and strong deflection of the solar wind beam. Starting just after 00:40:00 UT, both the magnetic field strength and ion and electron density experienced an enhancement up to ~ 5 nT (field) and ~ 2 cm^{-3} (densities) lasting ~ 5 s. After this, both the field strength and density dropped to below pre-event levels (~ 1 nT and 0.5 cm^{-3}) for ~ 10 s. Corresponding to this time, the ion and electron temperatures were clearly

enhanced again (up to ~ 500 eV for ions and ~ 16 eV for electrons). Also, the ion velocity was deflected, with ~ 100 km/s enhancements in V_Y and V_Z and a decrease in V_X by up to 400 km/s. These features were followed by another enhancement of magnetic field strength and density above the previous enhanced level between $\sim 00:40:40$ and $00:41:00$ UT, when the temperatures drop and ion velocity returned to closer to the pre-event direction. Another cavity region in the magnetic field strength and density followed this, after $\sim 00:41:00$ UT, and the event ended with a final compression region, in which the field strength and density reached their

highest levels of the period (i.e., ~ 6.5 nT and between 3 and 4 cm^{-3}). The electron temperature remained enhanced through this period, which is consistent with the enhancements in electron flux at energies between 500 eV and 2 keV, and there was a slight velocity deflection associated with the second cavity and final compression regions. Based on the presence of suprathermal ions throughout the event, these features were clearly related to the ion foreshock, which is consistent with the dominant component of the field being in the X_{GSM} direction during the event.

5.2.2. Analysis

[37] Because this event was associated with two rotations in the IMF, we calculated normal directions associated with each. MVA revealed good-fit normal directions of $[0.57, -0.68, -0.47]$ ($\lambda_3/\lambda_2 = 0.02$) and $[0.26, -0.88, -0.40]$ ($\lambda_3/\lambda_2 = 0.02$), both in GSM, for the rotations observed by TH-B between 00:37:50–00:38:10 UT and 00:38:45–00:39:00 UT, respectively. Cross-product analysis revealed slightly different directions, $[0.41, -0.49, -0.76]$ for the first rotation and $[0.41, -0.46, -0.79]$ for the second, though these are oriented similarly to those from the MVA. Because of the good fits and the complication for cross-product analysis due to two discontinuities in close succession, we used the MVA analyses for the following characterization tests. B_N remained finite and continuous through both discontinuities, so these were likely rotational discontinuities. Based on the orientations, the discontinuities were already connected to the bow shock when they were observed at both TH-B and TH-C, and the convection electric fields were pointed back into the discontinuities on their downstream sides. As observed by TH-C, there were two cavity regions flanked on either side by compressions and sharing a common compression region in the middle. These cavities corresponded to the two rotations observed in the IMF. Particularly in the first core region (centered around $\sim 00:40:20$ UT), the plasma temperature was significantly heated and the ion velocity deflected. Performing coplanarity analysis on the trailing (i.e., upstream) compression region (more shock-like) associated with the second cavity revealed a normal direction of $[0.33, 0.84, -0.42]$, which has its strongest component in the Y_{GSM} direction (i.e., approximately perpendicular to the local bow shock normal direction, see Figure 4). MVA revealed an unstable, poorly fit normal direction of $[0.57, 0.82, 0.00]$ in GSM with $\lambda_3/\lambda_2 = 0.67$; the unstable, poor fit may also have resulted from the lack of high-resolution data. The features of this event are all consistent with those of HFAs, indicating that both of the rotations in this short period developed HFAs when they interacted with the bow shock. Assuming motion along the bow shock, the sizes of these events were $2.7 R_E$ and $1.1 R_E$ in the directions parallel to their respective discontinuity normal directions.

[38] Summarizing, classic HFA-like structures were observed corresponding with each discontinuity observed at TH-C. The formation criteria for HFAs were satisfied for both discontinuities, and the observations confirm characteristics consistent with the passage of two HFAs. Both discontinuities were already connected to the bow shock prior to event observation (criterion 1), and both satisfied the convection electric field condition (criterion 5). The sizes and apparent motion are consistent with criteria 3 and 4 for HFAs. Compression regions formed on both sides of each event (criterion 6), with the upstream side forming into a shock-like structure with a

normal direction approximately perpendicular to the bow shock normal, consistent with the expected geometry for an HFA at this location (criterion 7). Furthermore, consistent with our understanding of HFA structure based on hybrid simulations, such HFA-like signatures were not observed upstream at TH-B, despite the discontinuities already being connected to the bow shock for some time prior to being observed there (in particular, the second discontinuity was connected long before being observed at TH-B).

5.3. Foreshock Bubble Example 3

5.3.1. Observations

[39] During this final period of interest, TH-B was in the ion foreshock from the beginning of the period (22:25:00 UT) until between $\sim 22:31$ and 22:32 UT, when the spacecraft passed through the foreshock compressional boundary (FCB on Figure 9) and the fluxes of suprathermal ions observed by the SST instrument returned to background levels (black color in Figure 9, i^+ eFlux). This indicates that there was some rotation of the IMF significant enough to change the foreshock. However, TH-B also observed very distinct ULF and nonlinear wave signatures while it was in the foreshock; these waves may have masked the discontinuity, as is shown in the hybrid simulation results in Figure 3a. These waves were probably also responsible for the abundance of energetic ion and electron flux during this period, because they are particularly effective at scattering and reflecting particles back toward the bow shock (i.e., first-order Fermi acceleration) [e.g., Jokipii, 1965].

[40] THEMIS-C also observed enhanced ULF and nonlinear waves in the ion foreshock during the first five minutes of the period shown in Figure 9. Starting around 22:30 UT, TH-C observed a decrease in total field strength and density and an increase in ion temperature. These signatures became more pronounced starting at $\sim 22:30:30$ UT, when a significant deflection of the ion velocity was also observed. By $\sim 22:30:55$ UT, the ion temperature was >1300 eV and the velocity was sunward. Just before 22:31:00 UT, TH-C observed a shock-like structure, characterized by a very strong enhancement in total field strength (up to ~ 20 nT) and density (up to $2\text{--}3 \text{ cm}^{-3}$; note that the density spike might not have been fully captured due to insufficient temporal resolution of the ESA instrument at this time). Following this, TH-C also passed through the foreshock compressional boundary and into pristine solar wind after $\sim 22:33$ UT (not shown in Figure 9), further demonstrating that there was some rotation of the IMF.

5.3.2. Analysis

[41] Because the IMF discontinuity associated with this event was probably masked by the wave activity in the foreshock, it is impossible to determine a discontinuity orientation. Using the average TH-B field direction between 22:25 and 22:29 UT compared to that during 22:32–22:36 UT, the IMF rotated by 23° . Without observations of the discontinuity itself though, the amount of tests we can perform on this event are limited, though here we demonstrate how the remaining identification criteria can still be used to determine if the observations are more consistent with an HFA or an FB. Assuming motion with the solar wind, at TH-C, the event would have been $\sim 6 R_E$ parallel to the X_{GSM} direction. Note that there was not a distinct compression region on the downstream side of the event, and indeed, when the reflected-to-incident density ratio was examined just before

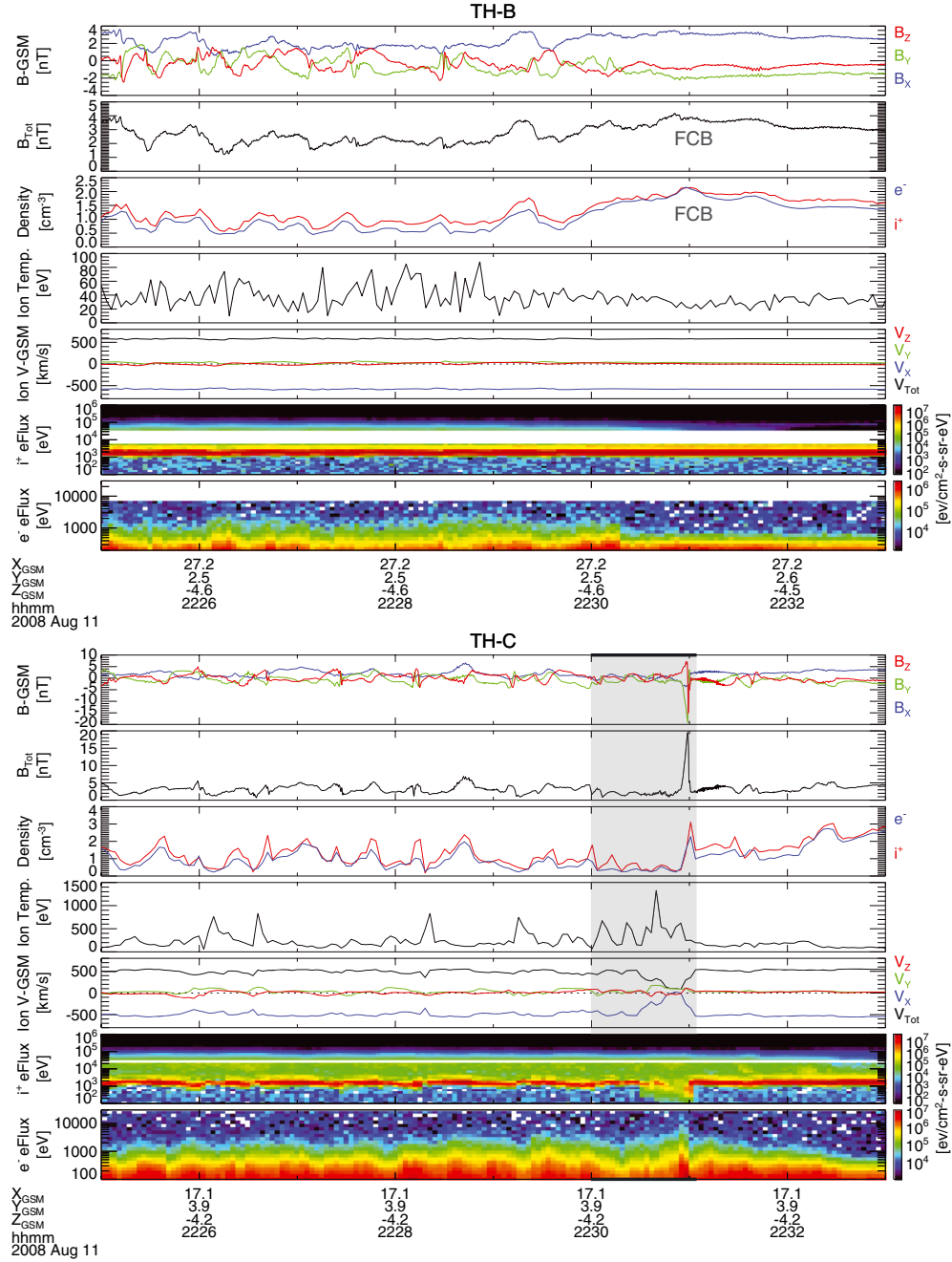


Figure 9. TH-B (top) and TH-C (bottom) observations during the third FB example period: 22:25–22:33 UT on 11 August 2008. The format is the same as described in Figure 5. Note that the TH-B ESA was in solar wind mode, and the ion temperature in the pristine solar wind from OMNI was ~ 20 eV during this period.

22:30 UT, it revealed that the ratio was less than 0.1, meaning that an HFA forming under these conditions should have developed a downstream compression region. The upstream shock might have originally been interpreted as a short large-amplitude magnetic structure event [e.g., *Schwartz and Burgess, 1991*], but when combined with our new understanding of FBs and the observations of the low-field-strength, tenuous, super-heated, and highly deflected core region just downstream, this shock is most consistent with that forming upstream of a transient foreshock event. Coplanarity analysis on this shock reveals a normal

direction of $[0.91, -0.38, -0.16]$ in GSM, but MVA reveals a good-fit normal direction of $[0.32, -0.93, -0.16]$ in GSM ($\lambda_3/\lambda_2 = 0.02$ using the period 22:30:58–22:31:03 UT). Thus, the direction of the upstream shock is inconclusive. Summarizing, the discontinuity that may have been responsible for generating this event is not clear in either the TH-B or -C observations. However, the size and lack of a downstream compression region are both consistent with characteristics of an FB. The lack of significant electron heating and relatively small size (compared to the other FB examples shown here) may

indicate that this FB was not well developed when it was observed at TH-C.

6. Discussion

[42] Here we have analyzed observations of five transient foreshock events using simultaneous TH-B and -C observations upstream of Earth's bow shock. Table 1 summarizes the results of these analyses, which employed the identification criteria defined in section 2. There are several key differences between the FBs and HFAs observed by TH-B and -C described here. These differences can be clearly explained with the observations from 14 July 2008. First, the upstream spacecraft, TH-B observed evidence of the foreshock in both cases, but only for the FB observations did it observe core-like signatures (depressed field strength and tenuous, hot plasma). This shows that the FB had already started to form when the discontinuity was observed at TH-B. Based on simulations of both FBs and HFAs [e.g., *Omidi et al.*, 2010; *Omidi and Sibeck*, 2007], the features of HFA cores should be mostly diminished as far upstream as TH-B was at the time of the observations, but an FB could have already started forming. The FB was probably in its early stages of development when it was observed at TH-B because there was no evidence of a shock at the upstream edge of the event. Next, in the FB observation at 21:58 UT, TH-C observed a clear core region, consisting of field strength and density depletions, enhanced temperatures up to a couple thousand eV, and sunward plasma velocity, followed by an upstream shock, with field strength >20 nT, density >10 cm $^{-3}$, corresponding to a strong pressure imbalance. Figure 10a shows a zoomed-in view of the FB observations by TH-C, with the key features discussed here labeled. Timing analysis between the two spacecraft shows that *this event was moving with the solar wind, not along the bow shock*. Note also that there was no shock or evidence of a compression region on the downstream side of the core features. This is consistent with TH-C passing from the foreshock into the core of an FB, as illustrated in Figure 3b (yellow arrow 1). Figure 3b also shows an alternate scenario in which an FB may be observed with two compression regions flanking the core; this can occur if a spacecraft passes through the lobe of an FB. Such a scenario may closely resemble the expected characteristics of an HFA, and this demonstrates why care must be taken to examine all of the identification criteria, preferably using multiple spacecraft, to distinguish between the two phenomena.

[43] THEMIS-C's observations of the HFA on Bastille Day 2008 (see Figure 10b for a zoomed-in view with key features labeled) were notably different than those of the FBs presented here; it observed two distinct compression regions flanking the core and the first IMF discontinuity. This is consistent with the picture of an HFA core expanding into and compressing the plasma around it as it moves *along the bow shock, not with the solar wind*. These compression regions are not full shocks, as is evident from the continuous variation and low field strength and density peaks compared with pre-event levels. These compression regions can evolve into shocks on one or both sides of HFAs depending on how the HFA is moving along the bow shock with respect to the incident solar wind [e.g., *Thomsen et al.*, 1988]. A caveat

Table 1. Summary of Event Analyses Using the HFA or FB Identification Criteria Defined in Section 2

Classification Criteria:	Event					
	14 July 21:58 UT	14 July 22:28 UT	11 August 05:09 UT	11 August 22:31 UT	12 August 00:41 UT	
1. IMF discontinuity intersects the bow shock?	Yes	Yes	Yes	Yes	Yes	
2. Is event upstream, centered around, or downstream of the IMF discontinuity?	Upstream	Centered around	Upstream	?	Centered around/ downstream	
3. Estimated size:	7–9 R_E	4.8 R_E	10 R_E	6 R_E	1.1–2.7 R_E	
4. Estimated motion:	With solar wind	Along bow shock	With solar wind	With solar wind	Along bow shock	
5. Electric field points back into the IMF discontinuity?	Yes	Yes	Yes	?	Yes	
6. If compression/shock on only one side, what is the reflected-to-incident ion density ratio?	< 0.1	N/A	~ 0.1	< 0.1	N/A	
7. Angle between the upstream compression or shock normal and GSM-X:	18°	60°	24°	?	70°	
Conclusion:	FB	HFA	FB	FB	HFA	

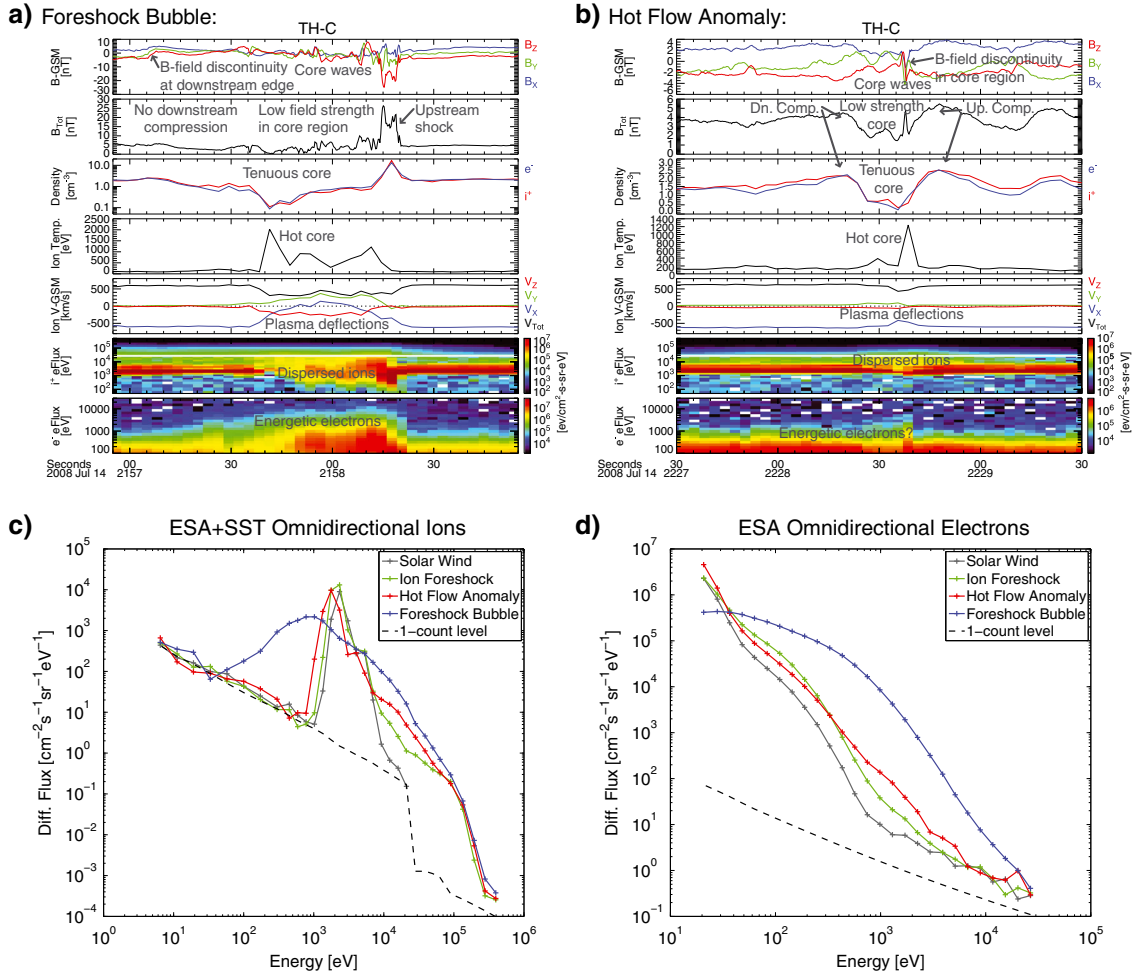


Figure 10. Direct comparison of the first FB and HFA examples, including particle distributions from different plasma regions: (a) Enhanced view of the foreshock bubble observed by TH-C on 14 July 2008 (see also Figure 5). (b) Enhanced view of the HFA observed by TH-C at ~22:28:30 UT on the same day (see also Figure 6). In both Figures 10a and 10b, characteristic regions and features are labeled. (c) Ion omnidirectional energy-flux distributions in the spacecraft frame for four different plasma regimes, all observed on 14 July 2008 by TH-C. Distributions are taken from the pristine solar wind between 22:50:30 and 22:51:00 UT, the ion foreshock between 21:59:45 and 22:00:15 UT, the core of the HFA shown in Figure 10c between 22:28:30 and 22:28:45 UT, and the core of the FB shown in Figure 10a between 21:58:00 and 21:58:15 UT. (d) Same as shown in Figure 10c but for electrons.

that should be noted here is that the HFA observed by TH-C on Bastille Day may have been a “young” HFA, i.e., not fully developed [Zhang *et al.*, 2010]. A fully developed HFA may have a hotter core temperature, more strongly deflected flows, and a shock on one or both sides. The double-HFA on 12 August, however, was probably well-developed based on the discontinuity’s connectivity time to the bow shock and the presence of energetic electrons and a shock on the upstream edge, and this event shares all of the same expected characteristics of HFAs as the event from Bastille Day. Both of these example HFA events also reveal how HFA features diminish rapidly away from the bow shock, because they are not observed $>10 R_E$ upstream by TH-B despite connectivity to the bow shock.

[44] Two of the most distinguishable differences in the HFA and FB examples here are the variations in ion velocities and the energetic electron population associated with each of these events. As previously mentioned, the electrons

at energies between 0.5 and 10 keV were enhanced by up to 2 orders of magnitude in the core regions of two of the three example FBs. Although the HFAs were associated with some enhanced energetic electron fluxes, the magnitude (less than one order of magnitude) and energy range (up to only a couple keV) are inconsistent with what was observed for the FBs (2 orders of magnitude up to ~10 keV). This is because the acceleration mechanisms for the two events are probably quite different. FBs are associated with two shocks: the original shock responsible for the foreshock formation (e.g., Earth’s bow shock for these cases) and the shock that forms at the FB’s upstream edge. These shocks converge as an FB convects antisunward with the upstream plasma. Furthermore, the presence of enhanced wave activity within FBs results in additional particle scattering and reflections. Thus, FBs create ideal conditions for Fermi acceleration and shock-drift acceleration of solar wind and foreshock particles [Omidi *et al.*, 2010]. The scenario is

entirely different for the expanding, suprathermal ion cores of HFAs, and from the observations presented here, there is a difference in the potential for particle acceleration between HFAs and FBs, particularly so for electrons.

[45] Figures 10c and 10d also show example omnidirectional flux-energy distributions from four different plasma regimes (solar wind, ion foreshock, HFA core, and FB core) observed within the same period by TH-C on Bastille Day. The HFA and FB events are the same as those shown as examples here. The solar wind beam is visible in the solar wind, foreshock, and HFA ion distributions as the peak in flux between ~ 1 and 3 keV. Note however, that both the foreshock and the HFA exhibit enhanced fluxes of ions (>10 keV) and electrons (all energies) compared to the pristine solar wind. Additional heating is evident within the HFA core by the enhancement of energetic particle flux compared to those in the ion foreshock. Within the FB core, both the ion and electron fluxes were enhanced at higher energies (up to ~ 200 keV for ions and ~ 10 keV for electrons). The high-energy cutoffs associated with the FB events likely result from the finite spatial scales of the FB shock and bow shock; once particle gyroradii grow to similar spatial scales, they will no longer be magnetically confined by the converging shock system. This picture is also consistent with the higher energy threshold (relative to that in the solar wind frame) for electrons, due to their much smaller gyroradii compared to ions of the same energy. Also in the FB core, the ion solar wind beam (i.e., the coherent beam seen at a few keV in the ion energy flux spectra and energy distribution) is fully dispersed, resulting in the spread in ion energy seen in the ion distribution. Note too that in the spacecraft frame, the plasma in the FB core was moving slower, explaining the ion peak moving to lower energy, but the temperature was much hotter, consistent with the significant spread in the distribution. HFAs should also be able to fully disrupt the ion solar wind beam, but their potential and exact mechanisms for heating electrons are still not well understood. However, it should be noted again that this might not have been a fully developed HFA. The exact mechanism responsible for electron heating in HFAs remains an unanswered question, though wave particle interactions [Zhang *et al.*, 2010] and/or reconnection [Hasegawa *et al.*, 2012] may play a role; additional studies are needed to statistically quantify and understand electron heating in HFAs.

[46] Many important outstanding questions remain concerning foreshock bubbles. The simulations of Omid *et al.* [2010] only examined their formation upstream of rotational discontinuities, and whether or not FBs can be generated by tangential discontinuities remains untested. However, the second FB case shown here was possibly associated with a tangential discontinuity. For an FB to form upstream of a tangential discontinuity, the width of the discontinuity would have to be thin enough to allow the suprathermal ions to pass through it (i.e., thinner than the suprathermal ions' gyroradii), because magnetic fields do not connect the upstream and downstream plasmas. Concerning magnetosheath dynamics, ripples and disturbances on the quasi-parallel bow shock can result in supermagnetosonic jets forming in the sheath [Hietala *et al.*, 2009; Archer *et al.*, 2012], and observations confirm that such jets occur regularly in the subsolar sheath during radial IMF [Plaschke *et al.*, 2012]. Because transient

foreshock phenomena, like FBs and HFAs, result in large deformations of the bow shock, their role in generating these jets should be investigated. It is understood that HFAs can have significant impacts on the magnetosphere-ionosphere system [e.g., Eastwood *et al.*, 2008; Jacobsen *et al.*, 2009], but the impacts of FBs have yet to be examined or quantified. FBs are expected to result in globally observable effects [Omid *et al.*, 2010], from sudden and drastic magnetopause motion, compressional waves, and ionospheric disturbances related to field-aligned current systems. Finally, because collisionless shocks in magnetized plasmas are known to occur throughout the Universe (e.g., Earth's and other planetary bow shocks, the heliospheric bow shock and those around other stars, and supernovae), FBs should occur at quasi-parallel shocks where the upstream magnetic field exhibits discontinuous behavior. Net particle acceleration relates to the system scale size, the converging shocks' relative velocity, and incident particle distributions. Thus, the potential for FBs to accelerate particles at various astrophysical shocks is high and entirely unexplored.

[47] We conducted a preliminary survey of the THEMIS dayside phase from 2008 (14 July to 15 October 2008). During this period, we identified 176 HFA-like events, 62 FB-like events, and 45 that were not easily classified as either. These events are only from the period of time when both TH-B and -C were simultaneously upstream of the bow shock, which is only satisfied around 44% of the time in the period. Exact classification of all of the identified events using analysis like that presented for the example events here is still ongoing, yet preliminary statistics can be presented. Based on the observations and accounting for the simultaneous coverage time, HFA-like events occur ~ 4 times per day, while FB-like events only occur ~ 1 time per day. However, when the solar wind speed was greater than 500 km/s, these occurrence rates increase to 12 HFA-like events per day and 5 FB-like events per day. By comparison, when the solar wind speed was less than 500 km/s, these occurrence rates drop to 2 per day for HFAs and 0.2 per day for FBs (only 5 FB-like events were observed for $V_{sw} < 500$ km/s). Note that these rates do not correct for those days when TH-B and -C were not in the ion foreshock and thus, unable to identify foreshock phenomena. These preliminary statistics demonstrate that these large-scale, transient foreshock phenomena occur regularly. Many days in the period proved to be particularly active, with 14–15 July producing 62 distinct transient events and 11–12 August producing 32. Also, the survey revealed that FBs tend to occur in groups, as in the first example period from Bastille Day discussed here. The activity observed by TH-B and -C between 21:52 and 21:57 UT is also consistent with FBs, revealing that three may have occurred during this 8 min interval. From the survey results, closely grouped “trains” of two or more FBs may occur regularly under the appropriate conditions. We speculate that these may result due to rotational discontinuities occurring in close succession and interacting with the new foreshock regions that can develop upstream of FB shocks (see Figure 3b as an example). This is yet another outstanding question concerning FBs, left here for future examination.

7. Conclusion

[48] Using multipoint THEMIS data, we presented the first observations of foreshock bubbles, a kinetic

phenomenon that can form when an IMF discontinuity interacts with backstreaming energetic ions in Earth's foreshock region. Conditions for FB formation are commonplace, and thus, it is likely that prior observations of such structures were not duly appreciated due to the remarkable similarities between in situ observations of HFAs and FBs. For example, see the special subset of events identified in Paschmann *et al.* [1988] as "single-sided" cases, where shocks or compression regions were only identified on the trailing edges (i.e., upstream sides assuming FB-like motion with the solar wind) of the events. In future studies, careful analysis, preferably using multiple spacecraft, should be conducted to properly distinguish HFAs from FBs. Here, we have introduced seven features that distinguish these two types of transient foreshock events and demonstrated their use as identification criteria. Preliminary statistics from an ongoing study of multiple HFA and FB events reveal that these events occur regularly, multiple times per day, particularly during above average solar wind speed. FBs should result in global-scale magnetospheric disturbances, and a follow-up study in progress will investigate the effects of FBs on the magnetosphere-ionosphere system. Finally, we have attributed enhanced fluxes of energetic particles seen in and near FBs as evidence for acceleration via Fermi and shock-drift acceleration processes, which should occur as the FB shock converges upon the bow shock. The observations presented here provide direct measurements of both ions and electrons accelerated by converging shocks in FBs at Earth. One key difference between HFAs and FBs may be the energy threshold to which energetic electrons can be accelerated: two of the three FBs examined here were accompanied by electron enhancements at energies up to ~ 10 keV, while the HFAs examined revealed electron enhancements up to only ~ 2 keV. Comparisons of observations from THEMIS and models can ascertain FB properties, including their efficacy in energetic particle generation, before applying the knowledge gained to other astrophysical settings.

[49] **Acknowledgments.** D. L. Turner thanks Ferdinand Plaschke, Michael Hartinger, and Heli Hietala for invaluable discussions, comments, questions, and suggestions. The authors would all like to thank the entire THEMIS team and especially the following people for providing various instrument data: Karl-Heinz Glassmeier (spacecraft magnetometers), Jim McFadden (ESA), and Davin Larson (SST). This work was funded under NASA contract NAS5-02099, and N. Omididi acknowledges NSF grant AGS-1007449.

References

- Angelopoulos, V., et al. (2008), First results from the THEMIS mission, *Space Sci. Rev.*, **141**, 453–476.
- Archer, M. O., T. S. Horbury, and J. P. Eastwood (2012), Magnetosheath pressure pulses: Generation downstream of the bow shock from solar wind discontinuities, *J. Geophys. Res.*, **117**, A05228, doi:10.1029/2011JA017468.
- Auster, H. U., et al. (2008), The THEMIS fluxgate magnetometer, *Space Sci. Rev.*, **141**, 235–264.
- Berchem, J., and C. T. Russell (1982), Magnetic field rotation through the magnetopause: ISEE 1 and 2 observations, *J. Geophys. Res.*, **87**, No. A10, 8139–8148.
- Eastwood, J. P., E. A. Lucek, C. Mazelle, K. Meziane, Y. Narita, J. Pickett, and R. A. Treumann (2005), The Foreshock, *Space Sci. Rev.*, **118**, 41–94.
- Eastwood, J. P., et al. (2008), THEMIS observations of a hot flow anomaly: Solar wind, magnetosheath, and ground-based measurements, *Geophys. Res. Lett.*, **35**, L17S03.
- Facsco, G., K. Kecskemety, G. Erdos, M. Tatallyay, P. W. Daly, and I. Dandouras (2008), A statistical study of hot flow anomalies using Cluster data, *Adv. Space Res.*, **41**, 1286–1291.
- Fairfield, D. H. (1971), Average and unusual locations of Earth's magnetopause and bow shock, *J. Geophys. Res.*, **76**, 6700–6716.
- Fuselier, S. A. (1995), Ion distributions in the Earth's foreshock upstream from the bow shock, *Adv. Space Res.*, **15**, 43–52.
- Giacalone, J. (1992), Shock drift acceleration of energetic protons at a planetary bow shock, *J. Geophys. Res.*, **97**, 8307–8318.
- Hasegawa, H., H. Zhang, Y. Lin, B. U. Ö. Sonnerup, S. J. Schwartz, B. Lavraud, and Q.-G. Zong (2012), Magnetic flux rope formation within a magnetosheath hot flow anomaly, *J. Geophys. Res.*, **117**, A09214, doi:10.1029/2012JA017920.
- Hietala, H., T. V. Laitinen, K. Andreeva, R. Vainio, A. Vaivads, M. Palmroth, T. I. Pulkkinen, H. E. J. Koskinen, E. A. Lucek, and H. Reme (2009), Supermagnetosonic jets behind a collisionless quasiparallel shock, *Phys. Rev. Lett.*, **103**, 245001(4).
- Jacobsen, K. S., et al. (2009), THEMIS observations of extreme magnetopause motion caused by a hot flow anomaly, *J. Geophys. Res.*, **114**, A08210.
- Jokipii, J. R. (1965), A model of Fermi acceleration at shock fronts with an application to the Earth's bow shock, *Astrophysical Journal*, **143**, 961–979.
- Lin, Y. (1997), Generation of anomalous flows near the bow shock by its interaction with interplanetary discontinuities, *J. Geophys. Res.*, **102**, 24265–24281.
- Lin, R. L., X. X. Zhang, S. Q. Liu, Y. L. Wang, and J. C. Gong (2010), A three-dimensional asymmetric magnetopause model, *J. Geophys. Res.*, **115**, A04207, doi:10.1029/2009JA014235.
- Masters, A., et al. (2009), Hot flow anomalies at Saturn's bow shock, *J. Geophys. Res.*, **114**, A08217.
- McFadden, J. P., C. W. Carlson, D. Larson, V. Angelopoulos, M. Ludlam, R. Abiad, B. Elliott, P. Turin, and M. Marckwardt (2008), The THEMIS ESA plasma instrument and in-flight calibration, *Space Sci. Rev.*, **141**, 277–302.
- Øieroset, M., D. L. Mitchell, T. D. Phan, and R. P. Lin (2001), Hot diamagnetic cavities upstream of the Martian bow shock, *Geophys. Res. Lett.*, **28**, 887–890.
- Omididi, N. and D. G. Sibeck (2007), Formation of hot flow anomalies and solitary shocks, *J. Geophys. Res.*, **112**, A10203.
- Omididi, N., D. G. Sibeck, and X. Blanco-Cano (2009), Foreshock compressional boundary, *J. Geophys. Res.*, **114**, A08205, doi:10.1029/2008JA013950.
- Omididi, N., J. P. Eastwood, and D. G. Sibeck (2010), Foreshock bubbles and their global magnetospheric impacts, *J. Geophys. Res.*, **115**, A06204.
- Paschmann, G., G. Haerendel, N. Sckopke, E. Mobius, H. Luhr, and C. W. Carlson (1988), Three-dimensional plasma structures with anomalous flow directions near the Earth's bow shock, *J. Geophys. Res.*, **93**, 11279–11294.
- Plaschke, F., H. Hietala, and V. Angelopoulos (2012), High speed jets in the subsolar magnetosheath: A statistical study, In preparation for *J. Geophys. Res.*
- Scholer, M., H. Kucharek, and K. J. Trattner (1998), Injection and acceleration of energetic particles at collisionless shocks, *Adv. Space Res.*, **21**, 533–542.
- Schwartz, S. J., et al. (1985), An active current sheet in the solar wind, *Nature*, **318**, 269–271.
- Schwartz, S. J. and D. Burgess (1991), Quasi-parallel shocks: A patchwork of three-dimensional structures, *Geophys. Res. Lett.*, **18**, 373–376.
- Schwartz, S. J. (1995), Hot flow anomalies near the Earth's bow shock, *Adv. Space Res.*, **15**, 107–116.
- Schwartz, S. J. (1998), Shock and discontinuity normal, Mach numbers, and related parameters, from Analysis Methods for Multi-Spacecraft Data, edited by G. Paschmann and P. W. Daly, 249–270.
- Shue, J.-H. et al. (1997), A new functional form to study the solar wind control of the magnetopause size and shape, *J. Geophys. Res.*, **102**, 9497–9511.
- Sibeck, D. G., T. D. Phan, R. P. Lin, R. P. Lepping, and A. Szabo (2002), Wind observations of foreshock cavities: A case study, *J. Geophys. Res.*, **107**, 1271.
- Sibeck, D. G., N. Omididi, I. Dandouras, and E. Lucek (2008), On the edge of the foreshock: model-data comparisons, *Ann. Geo.*, **26**, 1539–1544.
- Slavin, J. A. et al. (2009), MESSENGER and Venus Express observations of the solar wind interaction with Venus, *Geophys. Res. Lett.*, **36**, L09106.
- Sonnerup, B. U. O., and M. Scheible (1998), Minimum and maximum variance analysis, in Analysis Methods for Multi-Spacecraft Data, ISSI Sci. Rep. SR-001, edited by G. Paschmann and P. W. Daly, pp. 185–220, Eur. Space Agency Publ. Dif., Noordwijk, Netherlands.
- Thomas, V. A. and S. H. Brecht (1988), Evolution of diamagnetic cavities in the solar wind, *J. Geophys. Res.*, **93**, 11341–11353.
- Thomsen, M. F., J. T. Gosling, S. A. Fuselier, S. J. Bame, and C. T. Russell (1986), Hot diamagnetic cavities upstream from the Earth's bow shock, *J. Geophys. Res.*, **91**, 2961–2973.
- Thomsen, M. F., J. T. Gosling, S. J. Bame, K. B. Quest, C. T. Russell, and S. A. Fuselier (1988), On the origin of hot diamagnetic cavities near the Earth's bow shock, *J. Geophys. Res.*, **93**, 11311–11325.

- Turner, D. L., S. Eriksson, T. D. Phan, V. Angelopoulos, W. Tu, W. Liu, X. Li, W.-L. The, J. P. McFadden, and K.-H. Glassmeier (2011), Multispacecraft observations of a foreshock-induced magnetopause disturbance exhibiting distinct plasma flows and an intense density compression, *J. Geophys. Res.*, *116*, A04230.
- Zhang, H., D. G. Sibeck, Q.-G. Zong, S. P. Gary, J. P. McFadden, D. Larson, K.-H. Glassmeier, and V. Angelopoulos (2010), Time History of Events and Macroscale Interactions during Substorms observations of a series of hot flow anomaly events, *J. Geophys. Res.*, *115*, A12235.